PHYSICAL REVIEW E **85**, 035201(R) (2012)

Symmetry-induced pinning-depinning transition of a subharmonic wave pattern

Jeremías Garay, Ignacio Ortega, Marcel G. Clerc, and Claudio Falcón
Departamento de Física, Facultad de Ciencias Físicas y Matemáticas, Universidad de Chile, Casilla 487-3, Santiago, Chile

(Received 29 January 2011; revised manuscript received 19 July 2011; published 5 March 2012)

The stationary to drifting transition of a subharmonic wave pattern is studied in the presence of inhomogeneities and drift forces as the pattern wavelength is comparable with the system size. We consider a pinning-depinning transition of stationary subharmonic waves in a tilted quasi-one-dimensional fluidized shallow granular bed driven by a periodic air flow in a small cell. The transition is mediated by the competition of the inherent periodicity of the subharmonic pattern, the asymmetry of the system, and the finite size of the cell. Measurements of the mean phase velocity of the subharmonic pattern are in good agreement with those inferred from an amplitude equation, which takes into account asymmetry and finite-size effects of the system, emphasizing the main ingredients and mechanism of the transition.

DOI: 10.1103/PhysRevE.85.035201 PACS number(s): 05.45.−a, 47.20.Ky, 47.54.De, 47.55.Lm

Stationary to propagating transitions in pattern forming systems [1,2] have been studied theoretically, numerically, and experimentally in several examples, such as binary fluid convection [3], Faraday waves [4], and nonlinear optical patterns [5,6], to mention a few. However, this type of transition is usually studied in the context of spontaneous symmetry breaking [1], where the pattern will choose spontaneously the direction of its propagation as a control parameter η exceeds a critical value η_c. Another type of stationary to propagating transition arises when stationary patterns are exposed to induced parity-breaking effects, drift forces, or inhomogeneities, being commonly deformed and advected as $\eta < \eta_c$ [1,2], which are usually related to convective instabilities [1]. Although stationary to propagating transitions have been extensively studied (see [1] and references therein), to our knowledge there is no complete characterization of the effect of discreteness, finite size, or boundary effects. Furthermore, to our knowledge, no detailed study has been performed on the nature of the instabilities in finite-size domains for small η, such as in the case of secondary instabilities of cellular patterns. It has been observed in a nonlinear optical system [7], as in fluid convection experiments [3,8], that stationary patterns will not drift for small but nonzero η inside a definite range of values. Outside of this range, the patterns begin to drift. This phenomenon has been termed *pinning-depinning transition* [9]. This effect has been explained theoretically as a secondary imperfect bifurcation of stationary patterns to traveling waves due to spatial inhomogeneities [10]. However, as we will show later, the pinning-depinning transition is a generic phenomenon due to the coupling of envelope variations, generated by the boundary conditions and inhomogeneities, with the underlying pattern.

In this Rapid Communication, we study the stationary to drifting transition of subharmonic wave patterns in the presence of inhomogeneities and drift forces when the pattern wavelength is comparable with the system size. We understand the appearance of this transition as a competition between the inherent periodicity of the wave pattern, which acts as a potential barrier for the propagation of the oscillating pattern, and the asymmetry in the system, which induces a drift in a preferred direction. We study experimentally this type of transition of a subharmonic granular wave pattern in a small tilted container and we show the appearance of a pinning-depinning transition of the wave pattern as the inhomogeneity control parameter, i.e., the inclination angle of the container φ, is increased. We measure the mean phase velocity of the wave pattern and characterize the pinning range. In order to describe this type of transition, we propose a simple amplitude equation that describes correctly the evolution of the wave pattern, from which we derive a phase equation which trivially describes the transition, and we contrast it with numerical simulations and the experimental findings.

The prototype model used to describe phenomenologically the large-scale spatiotemporal dynamics in parametrically driven extended systems is the parametrically driven damped nonlinear Schrödinger equation with nonlinear dissipation [11,12],

$$\partial_\tau \psi = -i\nu\psi - (i+\delta)|\psi|^2\psi - i\partial_X^2\psi - \mu\psi + \gamma\bar{\psi}, \quad (1)$$

where $\psi(\tau,X)$ is an order parameter field that accounts phenomenologically for the envelope of the oscillatory surface of the wave patterns, and τ and X account for time and space coordinates, respectively. ν, μ, δ, and γ stand for the detuning between natural and forcing frequencies, linear and nonlinear damping, and parametric forcing amplitude, respectively. Nonlinear dissipation, proportional to δ, must be added in order to model the highly dissipative response of the system. The quiescent state $\psi = 0$ exhibits a spatial supercritical instability for positive detuning ($\nu > 0$) as energy injection equals energy dissipation ($\mu = \gamma$), generating patterns with an amplitude proportional to $\sqrt{\gamma - \mu}$ and a critical wave number $k_c \equiv \sqrt{\nu}$. Model (1) shows similar scenarios to those observed in parametrically amplified surface wave patterns.

To understand the presence of spatial inhomogeneities and drift forces, we introduce both effects in model (1) to correctly describe the wave pattern dynamics. More precisely, we consider that (i) the parameters become weakly inhomogeneous, i.e., $\tilde{\nu} = \nu + \epsilon\nu_o(X), \tilde{\mu} = \mu + \epsilon\mu_o(X)$, and $\tilde{\gamma} = \gamma + \epsilon\gamma_o(X)$, where the terms proportional to ϵ are small corrections, and (ii) a drift term develops on the wave pattern evolution. To account for these effects, the previous model is modified as

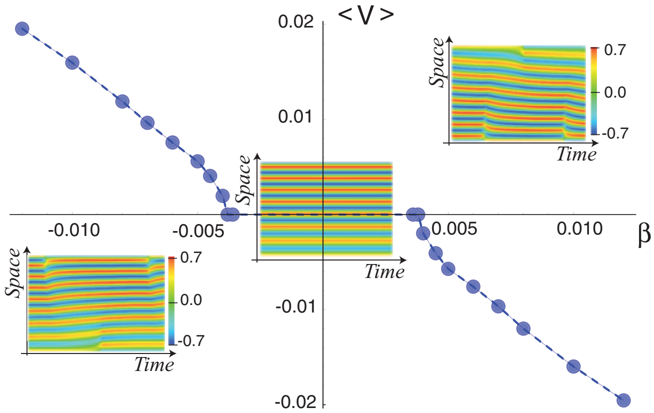

FIG. 1. (Color online) Pinning-depinning transition: bifurcation diagram of the mean pattern speed as a function of the intensity of drift for model (2) with $\tilde{\nu} = 0.058$, $\tilde{\delta} = 0.100$, $\tilde{\gamma} = 0.264$, and $\tilde{\mu} = 0.115$. The inset images correspond to the space-time evolution observed in the respective regions.

follows:

$$\partial_\tau \psi = -i\tilde{\nu}\psi - (i+\delta)|\psi|^2\psi - i\partial_X^2\psi - \tilde{\mu}\psi + \tilde{\gamma}\bar{\psi} + \beta\partial_X\psi, \tag{2}$$

where β accounts for the intensity of the drift. We can assume without loss of generality that $\nu_o(X)$, $\mu_o(X)$, and $\gamma_o(X)$ are proportional to X in the limit of a spatial linear ramp perturbation of the control parameter. The numerical simulations of model (2) with $\beta = 0$ and specular boundary conditions show stationary patterns with amplitude ($\sqrt{\tilde{\gamma} - \tilde{\mu}}$) and wave number ($\sqrt{\tilde{\nu}}$), which varies linearly along the system (cf. the inset of Fig. 1). It is noteworthy that for model (2) with $\beta = 0$, propagative patterns are not observed. This is understood by calculating the amplitude equation near the spatial instability, where only the modulus of the pattern amplitude is affected by inhomogeneities as it is deformed. Instead, the phase is not affected. Thus, the system cannot exhibit a pinning-depinning transition. On the other hand, numerical simulations considering only the drift term show a twofold effect: (i) the pattern is deformed as the amplitude increases in the direction of propagation (Fig. 1, insets), and (ii) for large enough β, we observe that the pattern propagates with constant speed. Figure 1 shows the behavior of the average speed as a function of β. When β is decreased, the pattern speed shows an oscillatory behavior (Fig. 1, right inset). By decreasing β even more, the pattern propagates through periodic jumps. The mean waiting time between jumps increases as β is decreased. Finally, for $\beta \leqslant \beta_c$ the pattern becomes stationary, i.e., it is nonpropagative, despite the fact that the system is in the presence of a drift force. In this region, termed *pinning range*, the pattern does not propagate. For negative β, we have an analog scenario, as illustrated in Fig. 1 (left inset). The origin of the pinning-depinning transition comes from the coupling between variations of the envelope and the underlying pattern, which in this case is caused by boundary conditions. This is similar to the phenomenon observed in front propagation [9,13]. To give a unified explanation of the pinning-depinning transition, let us consider the pattern near the spatial instability, with $\gamma = \mu + \Gamma$ ($\Gamma \ll 1$ is the bifurcation parameter) and the drift term, characterize by β, as a perturbation. Let us introduce in model (2) the following ansatz:

$$\psi(\tau,X) = \sqrt{\frac{\Gamma}{3\delta}}\cos[\sqrt{\nu}X + \phi(\tau,X)] + w(\phi,\tau,X), \tag{3}$$

where $\phi(\tau,X)$ stands for the phase of the pattern, which is a dynamic variable influenced by the drift force, and $w(\phi,\tau,X)$ accounts for the corrective terms, which are of the order of $\Gamma^{3/2}$. By linearizing in $w(\phi,\tau,X)$ in Eq. (2) after straightforward calculations, and using the stationary phase method for nonresonant terms [14], one finds the following phase equation at dominant order:

$$\partial_\tau\phi = \beta k_c + \partial_X\phi\kappa_o\sin(2\phi + 2k_cX), \tag{4}$$

where $\kappa_o = [\Gamma/2\delta^{1/3}]^{3/2}/k_c$. The first term describes the phase velocity induced by the drift. This speed is the usual result found using multiscale analysis. It is important to note that k_c is determined by the size of the system. The second term accounts for the coupling between the envelope variations and the underlying pattern: it is a spatial forcing proportional to the phase gradient, where the spatial variations of the envelope are comparable to the underlying pattern wavelength. This type of term emerges from nonresonant terms [13], which cannot be obtained using the standard multiscale method. Introducing the following change of variable, $\phi(\tau,X) = \chi(\tau) + \theta(X)$, where χ is the global phase and θ is a correction function, roughly proportional to X with small spatial oscillations [14]. By integrating over the spatial domain, the above equation reads

$$\dot{\chi} = \beta k_c + \beta_0 k_c \sin(2\chi + \chi_0), \tag{5}$$

where the dot stands for the time derivative, $\beta_0 \equiv \sqrt{a^2+b^2}/k_c$, $a = \kappa_o\int\partial_X\theta\cos(2\theta + 2k_cX)dx/L$, and $b = \kappa_o\int\partial_X\theta\sin(2\theta + 2k_cX)dx/L$, with L being the system size and $\tan(\chi_0) = a/b$. The dynamics of this global phase describes the motion of a pattern of a fixed amplitude which moves with a speed $\dot{\chi}$ driven by a constant forcing plus a periodic one. The bifurcation diagram of this equation is similar to that illustrated in Fig. 1, that is, for $|\beta/\beta_o| \leqslant 1$ (pinning range), the phase is constant that accounts for the stationary pattern, and for $|\beta/\beta_o| > 1$, the phase spreads by making a periodic movement that accounts for the traveling wave. One can integrate the above model and find the analytical expression for the average speed [15],

$$\langle\dot{\chi}\rangle = \begin{cases} -\frac{\beta}{\pi}\sqrt{(1/\beta_o)^2 - (1/\beta)^2}, & |(\beta/\beta_o)| > 1, \\ 0, & |(\beta/\beta_o)| \leqslant 1. \end{cases} \tag{6}$$

Hence, for small β, the pattern is stationary, and for $\beta = \beta_o$, the system exhibits a saddle-node bifurcation [9]. In the case of β greater than β_o, the pattern drifts with a speed that is proportional to the square root of β [$\langle\dot{\chi}\rangle \approx \sqrt{2(\beta - \beta_o)}$], and, finally, for large β, the pattern propagates with constant velocity proportional to β, which is consistent with the numerical observations illustrated in Fig. 1.

With the aim of studying a physical realization of this transition, we consider a shallow granular layer in a small cell subjected to a periodic air flow. The experimental cell and measurement techniques, displayed in Fig. 2, and the

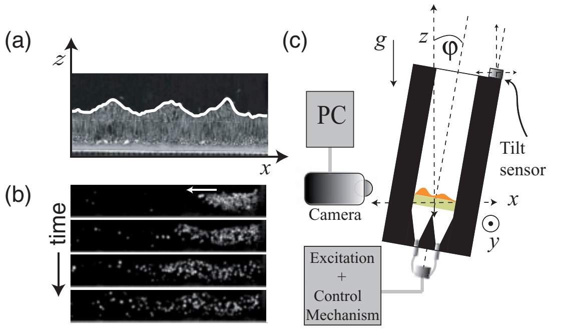

FIG. 2. (Color online) (a) Typical image used for interface tracking procedures. (b) Particle tracking scheme using fluorescent dyed particles. (c) Experimental setup as explained in Ref. [16].

theoretical description of the appearance of the large-scale pattern are similar to the one described in Ref. [16]. Here, the complex field ψ accounts for the envelope of the granular layer interface fluctuations [cf. Fig. 2(a)]. The periodic air flow is generated by an air compressor and regulated by an electromechanical proportional valve via a precision control regulator and an air lung. The aperture of the valve is controlled by a periodic voltage signal with a forcing frequency f_o coming from one of the outputs of a two-channel function generator through a power amplifier, and the pressure fluctuations generated by the air flow are monitored at 50 cm before the inlet by a dynamic pressure sensor and an oscilloscope. From the monitored pressure fluctuations, the peak pressure amplitude P_o is computed as the Fourier transform related to the forcing frequency f_o. The collective motion of the granular bed is acquired by a high-speed digital video camera triggered externally by the other output of the frequency generator. The acquisition frequency of the images is set at $f_o/2$ to ensure phase locking with the subharmonic wave pattern. The image sequence and its corresponding pressure signal are processed and analyzed. The granular surface profile is deduced by using an intensity threshold algorithm. Additionally, a biaxial tilt sensor driven by a 12 V power supply is positioned solidary on top of the cell in order to measure the inclination of the cell with respect to the axis of gravity in the x-z plane; this inclination is represented by the angle φ (cf. Fig. 2). In this experimental configuration, the angle φ of inclination is monitored by measuring the x-axis voltage difference. The variations of the off-plane inclination angle on the x axis are also monitored to ensure that only in-plane movements of the cell are allowed. Hence, for this experimental setup, the control parameters are the forcing frequency f_o, the peak amplitude P_o of the pressure fluctuations at f_o, and the in-plane inclination angle φ. The granular layer is deposited over a horizontal porous sponge and excited parametrically by a modulated air flow oscillating at $f_o = 10$ Hz at a peak amplitude P_o. Above a critical peak amplitude $P_o^c = 619 \pm 15$ Pa, a fluctuating stationary subharmonic wave pattern oscillating at half the forcing frequency, $f_o/2 = 5$ Hz, with a wavelength $\lambda_c = 2\pi/k_c = 1.2$ cm appears on the surface of the granular layer through a supercritical bifurcation. The amplitude of the wave pattern A_e is obtained from a set of images as P_o is varied. For a given value of P_o, the cell is inclined in the x-z plane with an angle φ. Both parameters can be related to Eq. (4) as $(P_o - P_o^c) \propto \Gamma$ and $\varphi \propto \beta$. In this configuration, the stationary subharmonic wave pattern suffers a secondary instability: it begins to *drift* to the left (right) for positive (negative) φ with a well-defined mean velocity $\langle v \rangle$ [cf. Fig. 3(a)]. The measured velocity of the pattern is computed as follows. For a given φ and peak pressure P_o^c, a set of images is acquired at $f_o/2$ for 200 s in a 600 × 400 px. From each image, the wave pattern is computed and filtered at the critical wavelength λ_c to compute its local unwrapped phase, $\phi(x,t) \approx k_c x + \chi(t)$ (as described above). As the pattern moves, we can compute the phase velocity of the pattern from the time derivative of χ, $\dot{\chi}$ [depicted in Figs. 3(b) and 3(c)], and then compute the mean velocity of the pattern by transforming phase changes to spatial changes through the

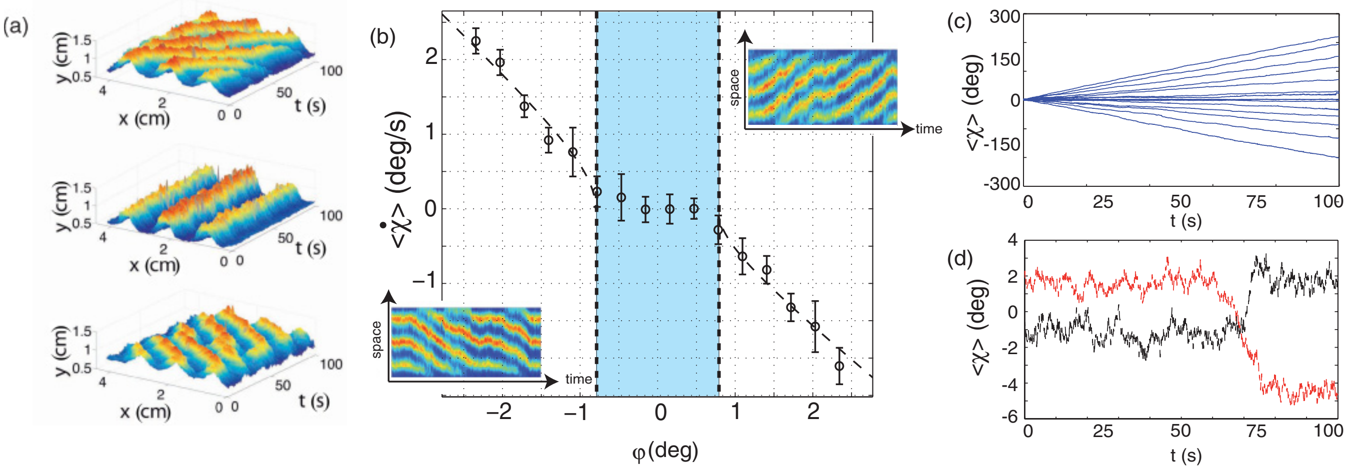

FIG. 3. (Color online) (a) Stroboscopic space-time diagrams acquired at $f_o/2$ of the subharmonic wave pattern for different inclination angles, $\varphi = -1.16^\circ$ (top), $\varphi = 0.15^\circ$ (middle), and $\varphi = 1.25^\circ$ (bottom). (b) Mean phase velocity $\langle \dot{\chi} \rangle$ vs inclination angle φ. The error bars correspond to the standard deviation of the measured velocity. The pinning range is depicted in blue (center column). Left (right) inset corresponds to the spatiotemporal diagram of the wave pattern amplitude for negative (positive) φ. (c) Temporal trace of the unwrapped global phase χ vs time t, for increasing φ (from top to bottom). (d) Temporal trace of the unwrapped global phase χ for $\varphi = 0.32^\circ$ (light gray) and $\varphi = -0.32^\circ$ (dark gray).

proportionality coefficient $r = 4$ s°/mm. The phase velocity $\langle \dot{\chi} \rangle$ (and hence the mean velocity of the pattern) is roughly proportional to φ for $|\varphi| > 1^\circ$, as shown in Fig. 3; however, as the inclination angle is decreased to small but measurable values, $|\varphi| \leqslant 0.8^\circ$, the mean velocity becomes rapidly zero and the pattern does not drift. This inclination interval, namely, the *pinning range* [9,13], is represented by the shaded region in Fig. 3(b). To emphasize the existence of a particle flow responsible for the pattern drift, we have performed a simple particle tracking scheme [cf. Fig. 2(b)]. Here, 20% of the grains are dyed with green fluorescent paint and placed at the left side of the cell. The layer is illuminated with UV lights and the fluorescent particles are tracked as they propagate through the layer. Using this technique, the mean velocity of the dyed particle center of mass $\langle v_d \rangle$ can be qualitatively described: $\langle v_d \rangle$ is larger as φ goes from positive to negative. Both the numerical and experimental results displaying a pinning-depinning transition of the subharmonic wave pattern present a good agreement with our theoretical prediction. In Fig. 3, the dashed curve is the fit obtained using Eq. (6) as a fitting curve: for small inclination φ, a pinning range develops [cf. Fig. 3(b)], and for φ larger than 1°, a linear tendency appears, with a slope ~ 1 (data not shown here). The inclusion of inhomogeneous coefficients does not change qualitatively the above description, but only slightly modifies the ansatz (3). The effect of noise and fluctuations can also be considered, rendering the transition smooth [13,14]. This effect is already observable in the mean velocity [cf. Fig. 3(b)], as experimental data show a clear smoothing of the pinning curve. To wit, a typical temporal trace of the unwrapped global phase is depicted in Fig. 3(d), where noise-induced phase jumps are shown for $\varphi = \pm 0.32^\circ$. These jumps are driven by fluctuations of the granular pattern, and can be understood from Eq. (5). In this sense, it must be stressed that this pinning-depinning phenomenon is independent of the system under study, and it can be found in other systems, where scale separation is broken by the coupling of large and small scales.

In conclusion, we have studied the pinning-depinning transition of stationary subharmonic waves in a quasi-one-dimensional fluidized shallow granular bed driven by a periodic air flow in a small cell. The transition is mediated by the competition of the inherent periodicity of the subharmonic pattern, the asymmetry of the system, and the finite size of the cell. The mechanism described above naturally emerges from the dynamic phase of the pattern when one considers the nonresonant terms.

M.G.C. and C.F. acknowledge the financial support of FONDECYT Grants No. 1090045 and No. 11090049, respectively, and the financial support of the ACT127 grant. C.F. acknowledges the financial support of FCFM, Universidad de Chile.

---

[1] M. C. Cross and P. C. Hohenberg, Rev. Mod. Phys. **65**, 851 (1993).
[2] R. E. Goldstein, G. H. Gunaratne, L. Gil, and P. Coullet, Phys. Rev. A **43**, 6700 (1991).
[3] D. R. Ohlsen, S. Y. Yamamoto, C. M. Surko, and P. Kolodner, Phys. Rev. Lett. **65**, 1431 (1990); D. R. Ohlsen *et al.*, J. Stat. Phys. **64**, 903 (1991); H. U. Voss, P. Kolodner, M. Abel, and J. Kurths, Phys. Rev. Lett. **83**, 3422 (1999).
[4] C. Godréche and P. Manneville, *Hydrodynamics and Nonlinear Instabilities* (Cambridge University Press, Cambridge, 1998).
[5] A. Petrossian *et al.*, Europhys. Lett. **29**, 209 (1995).
[6] U. Morgner and F. Mitschke, Phys. Rev. E **58**, 187 (1998).
[7] J. P. Seipenbusch, T. Ackemann, B. Schapers, B. Berge, and W. Lange, Phys. Rev. A **56**, 4401 (1997).
[8] I. Rehberg, E. Bodenschatz, B. Winkler, and F. H. Busse, Phys. Rev. Lett. **59**, 282 (1987).
[9] Y. Pomeau, Physica D **23**, 1 (1986).
[10] E. Knobloch, J. Hettel, and G. Dangelmayr, Phys. Rev. Lett. **74**, 4839 (1995).
[11] M. G. Clerc, S. Coulibaly, and D. Laroze, Phys. Rev. E **77**, 056209 (2008).
[12] E. Kenig, B. A. Malomed, M. C. Cross, and R. Lifshitz, Phys. Rev. E **80**, 046202 (2009).
[13] M. G. Clerc, C. Falcon, and E. Tirapegui, Phys. Rev. Lett. **94**, 148302 (2005); Phys. Rev. E **74**, 011303 (2006).
[14] U. Bortolozzo *et al.*, Adv. Nonlinear Opt. **2009**, 926810 (2009).
[15] F. Haudin *et al.*, Phys. Rev. Lett. **103**, 128003 (2009); Phys. Rev. E **81**, 056203 (2010).
[16] I. Ortega, M. G. Clerc, C. Falcon, and N. Mujica, Phys. Rev. E **81**, 046208 (2010).